General regularized boundary condition for multi-speed lattice Boltzmann models method

O. Malaspinas[c,a,*], B. Chopard[c], J. Latt[b]

[a] *Institut Jean le Rond d'Alembert - Université Pierre et Marie Curie, 4 place Jussieu - case 162, F-75252 Paris cedex 5, France*
[b] *Ecole Polytechnique Fédérale de Lausanne, , 1015 Lausanne, Switzerland*
[c] *Université de Genève, Comp. Sc. Dept, 1227 Carouge, Switzerland*

Abstract

The lattice Boltzmann method is nowadays a common tool for solving computational fluid dynamics problems. One of the difficulties of this numerical approach is the treatment of the boundaries, because of the lack of physical intuition on the behavior of the density distribution functions close to a wall. A massive effort has been made by the scientific community to find appropriate solutions for boundaries. In this paper we present a completely generic way of treating a Dirichlet boundary for two and three dimensional flat walls, edges or corners for weakly compressible flows and is applicable for any lattice topoogy. The proposed algorithm is shown to be second order accurate and could also be extended for compressible and thermal flows.

Keywords: lattice Boltzmann method, boundary conditions

1. Introduction

The lattice Boltzmann method (LBM) is a now commonly used solver in the field of computational fluid dynamics. It is applied to a wide range of physical phenomena ranging from Newtonian, non-Newtonian (see [1, 2, 3]), to multiphase and multi-component incompressible fluids (see [4]). Recent research has showed how to apply the LBM to compressible and thermal flows (see Shan *et al.* [5]).

One of the difficulties with the LBM is the boundary conditions (BC) treatment, since some populations are unknown and have therefore to be reconstructed in an ad-hoc manner. The community has developed a large variety of different algorithms that allow to model Dirichlet boundaries (see [6, 7, 8, 9] among others and a review of some of them can be found in [10]) and curved boundaries (see [11, 12, 13] for example). A problem of most of the current

*Corresponding author
Email addresses: orestis.malaspinas@gmail.com (O. Malaspinas), bastien.chopard@unige.ch (B. Chopard), jonas.latt@epfl.ch (J. Latt)

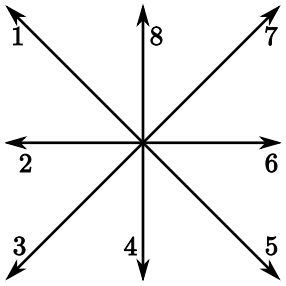

Figure 1: The D2Q9 lattice with the vectors representing the microscopic velocity set $\boldsymbol{\xi}_i$. A rest velocity $\boldsymbol{\xi}_0 = (0, 0)$ is added to this set.

state of the art approach is that interpolation is needed for geometries with corners and edges. In addition, no methodology has been proposed for multi-speed models, such as those containing up to 121 velocities in 3D.

In this paper we propose a completely generic way of handling any 2D and 3D on-lattice geometries (including corner and edges). Although in this paper we only discuss incompressible flows and nearest-neighbor lattices, our procedure il also valid for extended lattices (as those proposed in [5]) in the case hermal compressible flows. This article is organized as follows. In Sec. 2 the LBM is briefly described. In Sec. 3 the general regularized boundary condition (GRBC) is described. It is then benchmarked in Sec. 4 towards three 2D test cases, namely the Womersley and the dipole-wall collision flows and one 3D test case, the Poiseuille flow in a square duct. Finally we comment our results in Sec. 5.

2. Short lattice Boltzmann method introduction

The aim of this section is to remind the reader the basics of the LBM and to introduce the notations used throughout this work. For more details on the LBM, the reader should refer to [5, 1, 2, 14].

The LBM scheme for the BGK collision (for Bhatnagar, Gross, Krook [15]) is given by

$$f_i(\boldsymbol{x} + \boldsymbol{\xi}_i \Delta t, t + \Delta t) = f_i(\boldsymbol{x}, t) - \frac{1}{\tau}\left(f_i(\boldsymbol{x}, t) - f_i^{(0)}(\boldsymbol{x}, t)\right), \tag{1}$$

where f_i is the is the discrete probability distribution to find a particle with velocity $\boldsymbol{\xi}_i$ at position $\boldsymbol{x}$ at time t, $f_i^{(0)}$ is the discrete Maxwell–Boltzmann distribution, τ the relaxation time, and Δt the discrete time step. In this paper we are only interested in the weakly compressible case, therefore the discrete velocity set is given either by a D2Q9 (see Fig. 1)in 2D either by a D3Q15, D3Q19 or D3Q27 (see [5] for more details about lattices). The equilibrium distribution is given by

$$f_i^{(0)} = w_i \rho \left(1 + \frac{\boldsymbol{\xi}_i \cdot \boldsymbol{u}}{c_s^2} + \frac{1}{2c_s^4} \boldsymbol{Q}_i : \boldsymbol{u}\boldsymbol{u}\right), \tag{2}$$

where ρ is the density, $\boldsymbol{u}$ is the macroscopic velocity field, $\boldsymbol{Q}_i = \boldsymbol{\xi}_i\boldsymbol{\xi}_i - c_s^2\boldsymbol{I}$, c_s and w_i the lattice speed of sound and the lattice weights respectively. The density and the velocity fields are computed by the distribution through the relations

$$\rho = \sum_{i=0}^{q-1} f_i = \sum_{i=0}^{q-1} f_i^{(0)}, \tag{3}$$

$$\rho\boldsymbol{u} = \sum_{i=0}^{q-1} \boldsymbol{\xi}_i f_i = \sum_{i=0}^{q-1} \boldsymbol{\xi}_i f_i^{(0)}, \tag{4}$$

where q is the number of discrete velocities. Doing a multi-scale Chapman–Enskog (CE) expansion (see [16, 17] for more details) one can show that the LBM BGK scheme is equivalent to the incompressible Navier–Stokes equations

$$\boldsymbol{\nabla}\cdot\boldsymbol{u} = 0, \tag{5}$$

$$\partial_t\boldsymbol{u} + (\boldsymbol{u}\cdot\boldsymbol{\nabla})\boldsymbol{u} = -\frac{1}{\rho}\boldsymbol{\nabla}p + \nu\boldsymbol{\nabla}^2\boldsymbol{u}, \tag{6}$$

with $\nu = c_s^2(\tau - \frac{1}{2})$ being the kinematic viscosity and p the pressure.

The CE expansion is done under the assumption that f_i is given by a small perturbation of the equilibrium distribution

$$f_i = f_i^{(0)} + \varepsilon f_i^{(1)} + \mathcal{O}(\varepsilon^2), \tag{7}$$

where $\varepsilon \ll 1$ can be identified with the Knudsen number (see [18]).
One can also show that $f^{(1)}$ is given by

$$f_i^{(1)} = \frac{w_i}{2c_s^4}\boldsymbol{Q}_i : \boldsymbol{\Pi}^{(1)}, \tag{8}$$

where the tensor $\boldsymbol{\Pi}^{(1)} \equiv \sum_i \boldsymbol{\xi}_i\boldsymbol{\xi}_i f_i^{(1)}$ is related to the strain rate tensor, $\boldsymbol{S} = (\boldsymbol{\nabla}\boldsymbol{u} + (\boldsymbol{\nabla}\boldsymbol{u})^{\mathrm{T}})/2$ through the relation

$$\boldsymbol{\Pi}^{(1)} = -2c_s^2\rho\tau\boldsymbol{S}. \tag{9}$$

Therefore the f_i can be approximated by

$$f_i = w_i\rho\left(1 + \frac{\boldsymbol{\xi}_i\cdot\boldsymbol{u}}{c_s^2} + \frac{1}{2c_s^4}\boldsymbol{Q}_i : \boldsymbol{u}\boldsymbol{u}\right) + \frac{w_i}{2c_s^4}\boldsymbol{Q}_i : \boldsymbol{\Pi}^{(1)}. \tag{10}$$

3. Description of the general regularized boundary condition (GRBC)

In this section we assume that the velocity is prescribed on the boundary (Dirichlet boundary condition). This BC can be applied for flat walls or for corners. From the algorithmic point of view the LBM scheme is decomposed in two steps :

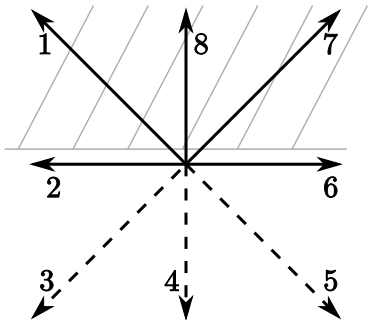

Figure 2: A boundary node for the D2Q9 lattice. The dashed arrows represent the unknown populations.

1. The collision

$$f_i^{\text{out}}(\boldsymbol{x},t) = \left(1-\frac{1}{\tau}\right) f_i(\boldsymbol{x},t) + \frac{1}{\tau} f_i^{(0)}(\boldsymbol{x},t). \tag{11}$$

2. The propagation

$$f_i(\boldsymbol{x}+\boldsymbol{\xi}_i, t+1) = f_i^{\text{out}}(\boldsymbol{x},t). \tag{12}$$

Therefore on a boundary node there are populations that are unknown before the collision since they are incoming from outside the computational domain as depicted on Fig. 2. Thus they have to be computed.

The idea is to compute all the unknown macroscopic moments, namely ρ and $\boldsymbol{\Pi}^{(1)}$, from the known f_is (using their expression 10), the velocity field and the equation for the density (see Eq. 3). We then construct a system of equations which is usually over-determined and solve it numerically.

We first define two sets of indices : the "known indices", $\mathcal{K}$, and the "unknown indices", $\mathcal{U}$, defined as

$$\mathcal{K} = \{i | f_i \text{ is known}\}, \quad \mathcal{U} = \{i | f_i \text{ is unknown}\}. \tag{13}$$

3.1. Construction of the linear system of equations

The first equation we use is the definition of ρ from Eq. 3

$$\rho = \sum_i f_i = \sum_{i\in\mathcal{K}} f_i + \sum_{i\in\mathcal{U}} f_i. \tag{14}$$

We then replace the unknown f_is by their CE expansion (see Eq. 10)

$$\begin{aligned}
\rho &= \rho_{\mathcal{K}} + \sum_{i\in\mathcal{U}} \left(\rho w_i g_i(\boldsymbol{u}) + \frac{w_i}{2c_s^4} \boldsymbol{Q}_i : \boldsymbol{\Pi}^{(1)} \right), \\
\rho_{\mathcal{K}} &= \rho \left(1 - \sum_{i\in\mathcal{U}} w_i g_i(\boldsymbol{u}) \right) + \left(\sum_{i\in\mathcal{U}} \frac{w_i}{2c_s^4} \boldsymbol{Q}_i \right) : \boldsymbol{\Pi}^{(1)}.
\end{aligned} \tag{15}$$

were we defined $\rho_{\mathcal{K}} \equiv \sum_{i\in\mathcal{K}} f_i$ and g_i as

$$g_i(\boldsymbol{u}) \equiv 1 + \frac{\boldsymbol{\xi}_i \cdot \boldsymbol{u}}{c_s^2} + \frac{1}{2c_s^4}\boldsymbol{Q}_i : \boldsymbol{u}\boldsymbol{u}. \tag{16}$$

The other equations are just given by the assumption that the known f_i are given by their CE expansion

$$\left\{ f_i = w_i \rho g_i(\boldsymbol{u}) + \frac{w_i}{2c_s^4}\boldsymbol{Q}_i : \boldsymbol{\Pi}^{(1)} \right\}_{i\in\mathcal{K}}. \tag{17}$$

This usually gives an over-determined system of equations for ρ and $\boldsymbol{\Pi}^{(1)}$. This system can be solved by a least squares problem as discussed hereafter. Once the density and $\boldsymbol{\Pi}^{(1)}$ are known, all the populations are recomputed using expression (10).

To illustrate the procedure we will consider a 2D flat boundary as depicted in Fig. 2. The two sets of indices, $\mathcal{K}$ and $\mathcal{U}$ are given by

$$\mathcal{K} = \{0, 1, 2, 6, 7, 8\}, \quad \mathcal{U} = \{3, 4, 5\}. \tag{18}$$

Thus the system of equations to solve will be

$$\underbrace{\begin{pmatrix} \rho_{\mathcal{K}} \\ f_0 \\ f_1 \\ f_2 \\ f_6 \\ f_7 \\ f_8 \end{pmatrix}}_{\boldsymbol{b}} = \underbrace{\begin{pmatrix} \frac{5}{6} + \frac{1}{2}u_y(1-u_y) & 0 & 0 & -\frac{1}{2} \\ \frac{4}{9} - \frac{2}{3}(u_x^2+u_y^2) & -\frac{2}{3} & 0 & -\frac{2}{3} \\ \frac{1}{36} - \frac{1}{12}(u_x - u_y - u_x^2 + 3u_xu_y - u_y^2) & \frac{1}{12} & -\frac{1}{4} & \frac{1}{12} \\ \frac{1}{9} - \frac{1}{6}(2u_x - 2u_x^2 + u_y^2) & \frac{1}{3} & 0 & -\frac{1}{6} \\ \frac{1}{9} + \frac{1}{6}(2u_x + 2u_x^2 - u_y^2) & \frac{1}{3} & 0 & -\frac{1}{6} \\ \frac{1}{36} + \frac{1}{12}(u_x + u_y + u_x^2 + 3u_xu_y + u_y^2) & \frac{1}{12} & \frac{1}{4} & \frac{1}{12} \\ \frac{1}{9} + \frac{1}{6}(2u_y - u_x^2 + 2u_y^2) & -\frac{1}{6} & 0 & \frac{1}{3} \end{pmatrix}}_{\boldsymbol{A}} \cdot \underbrace{\begin{pmatrix} \rho \\ \Pi_{xx}^{(1)} \\ \Pi_{xy}^{(1)} \\ \Pi_{yy}^{(1)} \end{pmatrix}}_{\boldsymbol{x}},$$

where $\rho_{\mathcal{K}} = f_0 + f_1 + f_2 + f_6 + f_7 + f_8$. The solution of this system can be found by solving the following minimization problem

$$\min ||\boldsymbol{A} \cdot \boldsymbol{x} - \boldsymbol{b}||. \tag{19}$$

This problem has as a solution of the form (see [19])

$$\boldsymbol{x} = (\boldsymbol{A}^{\mathrm{T}} \cdot \boldsymbol{A})^{-1} \cdot (\boldsymbol{A}^{\mathrm{T}} \cdot \boldsymbol{b}). \tag{20}$$

Similarly, one can construct a "mass conserving" boundary condition. Do do so it is only needed to replace Eq. (15) by the mass conservation constrain

$$\rho_{\mathrm{in}} = \rho_{\mathrm{in}}, \tag{21}$$

where ρ_{in} and ρ_{out} are defined as

$$\rho_{\text{in}} = \sum_{i \in \text{opp}(\mathcal{U})} f_i, \tag{22}$$

$$\begin{aligned}\rho_{\text{out}} &= \sum_{i \in \mathcal{U}} f_i^{\text{out}} = \sum_{i \in \mathcal{U}} \left[\left(1 - \frac{1}{\tau}\right) f_i(\boldsymbol{x}, t) + \frac{1}{\tau} f_i^{(0)}(\boldsymbol{x}, t) \right], \\ &= \sum_{i \in \mathcal{U}} \left[\left(1 - \frac{1}{\tau}\right) f_i^{(1)}(\boldsymbol{x}, t) + f_i^{(0)}(\boldsymbol{x}, t) \right], \end{aligned} \tag{23}$$

where $\text{opp}(\mathcal{U})$ stands for all indices of the microscopic velocities that are pointing in the opposite direction than those that are present in the $\mathcal{U}$ ensemble (in the case of Fig. 2 $\text{opp}(\mathcal{U}) = \{1, 7, 8\}$). Using Eq. (8) it is easy to put (21) is a form similar to Eq. (15)

$$\rho_{\text{in}} = \rho \left(\sum_{i \in \mathcal{U}} w_i g_i(\boldsymbol{u}) \right) + \left(1 - \frac{1}{\tau}\right) \left(\sum_{i \in \mathcal{U}} \frac{w_i}{2c_s^4} \boldsymbol{Q}_i \right) : \boldsymbol{\Pi}^{(1)}. \tag{24}$$

The method presented above can be used on two and three dimensional lattices for flat walls, edges and corners. The only limitation concerns the implementation of the corners for D3Q15 lattices since there are only 5 known f_is in such cases and therefore not enough information is available locally.

Finally it is possible to write a system of equations to impose pressure boundary conditions, but in this case the system will not be linear and therefore it will be much more difficult to solve.

3.2. Link with other boundary conditions

In this section we described a completely generic algorithm for implementing boundary conditions for flat walls edges and corners. We constructed an over-determined system of equations and solved it with a numerical method. A natural question would be to know if the number of equations could not be reduced by simple symmetry considerations to have as many equations as unknowns. In order to keep this discussion as simple as possible, we will again use the example of the preceding subsection of the wall depicted in Fig. 2. As in the preceding subsection we have four unknowns : ρ and $\boldsymbol{\Pi}^{(1)}$. The first equation used is expression (15). Then we are left with three constrains to be chosen freely. As before we will use Eq. (17) to close our system. But this time we will only select three f_is in order to end up with a total of four equations for four unknowns. From simple symmetry constrains we see that only four combinations of indices are possible

$$\mathcal{K}_{026} = \{0, 2, 6\}, \tag{25}$$

$$\mathcal{K}_{017} = \{0, 1, 7\}, \tag{26}$$

$$\mathcal{K}_{268} = \{2, 6, 8\}, \tag{27}$$

$$\mathcal{K}_{178} = \{1, 7, 8\}. \tag{28}$$

The system of equation to solve would then be

$$\rho_{\mathcal{K}} = \rho\left(1 - \sum_{i\in\mathcal{U}} w_i g_i(\boldsymbol{u})\right) + \left(\sum_{i\in\mathcal{U}} \frac{w_i}{2c_s^4}\boldsymbol{Q}_i\right) : \boldsymbol{\Pi}^{(1)},$$
$$\left\{ f_i = w_i\rho g_i(\boldsymbol{u}) + \frac{w_i}{2c_s^4}\boldsymbol{Q}_i : \boldsymbol{\Pi}^{(1)} \right\}_{i\in\mathcal{K}_j},$$

where the index j stands for 026, 017, 268 or 178. The systems with $\mathcal{K}_{268}$ and $\mathcal{K}_{126}$ have no solution since they contain no information about the off diagonal terms of the deviatoric stress tensor $\Pi^{(1)}_{xy}$. The two remaining systems yield the following solutions

$j = 017$:

$$\rho = (3/2)(4f_7 + f_0 + 4f_1)/(1 + u_y), \tag{29}$$
$$\Pi^{(1)}_{xx} = -(u_x^2 + (2/3)(u_y + 1))\rho + 2(f_6 + f_8 + f_2), \tag{30}$$
$$\Pi^{(1)}_{xy} = -(u_y + (1/3))\rho u_x - 2(f_1 - f_7), \tag{31}$$
$$\Pi^{(1)}_{yy} = (-u_y^2 + (1 - u_y)/3)\rho + 6(f_1 + f_7) - 2(f_2 + f_6 + f_8). \tag{32}$$

$j = 178$:

$$\rho = (2(f_7 + f_1 + f_8) + f_0 + f_2 + f_6)/(1 + u_y), \tag{33}$$
$$\Pi^{(1)}_{xx} = 4(f_1 + f_7) - 2f_8 - \rho u_x^2, \tag{34}$$
$$\Pi^{(1)}_{xy} = -(u_y + (1/3))\rho u_x - 2(f_1 - f_7), \tag{35}$$
$$\Pi^{(1)}_{yy} = -(u_y^2 + 1/3 + u_y)\rho + 2(f_1 + f_7 + f_8). \tag{36}$$

A first remark is that in the case of $j = 178$ we get the same value for the density ρ as the one found by the method used by Zou and He in [6]. Nevertheless, there is no way to make an a priori choice about the correct system to solve. We implemented both possibilities and the solution with $j = 017$ showed to be very unstable numerically. And therefore the solution yielding the "Zou-He"-like solution for the computation of the density must be chosen as the "correct" system to solve, which seems natural since this procedure is used for a long time to evaluate the density on boundary nodes.

We also see that there is no unique and consistent choice to *a priori* select the set of indices that one should use. Our approach therefore offers a completely generic alternative by solving the optimization problem of Eq. (19).

3.3. Extension to the multi-speed models

The LBM has been shown to be applicable in a very elegant fashion to thermal flows by extending the discrete velocity set at each lattice point (see [5]). In this framework, the neighborhood of each grid point is not anymore restricted to its nearest neighbors. This extension increases dramatically the number of

unknown f_is while adding only a very limited number of constrains. In 2D the there are 37 populations at each grid point (the number of unknowns for a flat wall is of 15). There are only 2 more constrains for a Dirichlet no slip wall, namely mass and energy conservation (which makes a total of four in 2D). Therefore the way of computing the density in a "Zou-He" fashion is not applicable anymore (see [6] for the "Zou-He" fashion of computing ρ on a wall). Our approach would be completely generic in this case too and the construction a system of equation similar of the one presented in Subsection 3.1 will remain similar. The Chapman–Enskog expansion of distribution functions are in this case given by

$$f_i^{(0)} = w_i \rho g_i(\boldsymbol{u}, \theta) + \frac{1}{2c_s^4} \boldsymbol{Q}_i : \boldsymbol{\Pi}^{(1)} + \frac{1}{6c_s^6} \boldsymbol{R}_i : \boldsymbol{T}^{(1)}, \tag{37}$$

where

$$\begin{aligned} g_i = \Bigg(& 1 + \frac{\boldsymbol{\xi}_i \cdot \boldsymbol{u}}{c_l^2} + \frac{1}{2c_l^4} \left[(\boldsymbol{\xi}_i \cdot \boldsymbol{u})^2 - c_l^2 \boldsymbol{u}^2 + c_l^2 (\theta - 1)(\xi_i^2 - c_l^2 D) \right] \\ & + \frac{\boldsymbol{\xi}_i \cdot \boldsymbol{u}}{6c_l^6} \left[(\boldsymbol{\xi}_i \cdot \boldsymbol{u})^2 - 3c_l^2 \boldsymbol{u}^2 + 3c_l^2 (\theta - 1)(\xi_i^2 - c_l^2 (D+2)) \right] \\ & + \frac{1}{24c_l^8} \Big[(\boldsymbol{\xi}_i \cdot \boldsymbol{u})^4 - 6c_l^2 \boldsymbol{u}^2 (\boldsymbol{\xi}_i \cdot \boldsymbol{u})^2 + 3c_l^4 \boldsymbol{u}^4 \\ & \quad + 6c_l^2 (\theta - 1) \left((\boldsymbol{\xi}_i \cdot \boldsymbol{u})^2 (\boldsymbol{\xi}_i^2 - c_l^2 (D+4)) + c_l^2 \boldsymbol{u}^2 (c_l^2 (D+2) - \boldsymbol{\xi}_i^2) \right) \\ & \quad + 3c_l^4 (\theta - 1)^2 \left(\boldsymbol{\xi}_i^4 - 2c_l^2 (D+2) \boldsymbol{\xi}_i^2 + c_l^4 D(D+2) \right) \Big] \Bigg), \end{aligned} \tag{38}$$

$\boldsymbol{R}_{\alpha\beta\gamma} \equiv \xi_\alpha \xi_\beta \xi_\gamma - c_s^2 (\xi_\alpha \delta_{\beta\gamma} + \xi_\gamma \delta_{\beta\alpha} + \xi_\beta \delta_{\alpha\gamma})$, and $\boldsymbol{T}^{(1)}$ is a fully symmetric rank three tensor. Therefore there will be for a flat wall case, 22 equations for each known f_is and two additional equations for mass and energy conservation, for a total of 24 equations for nine unknowns (the density, the temperature, $\boldsymbol{\Pi}^{(1)}$ and $\boldsymbol{T}^{(1)}$).

Furthermore the extended neighborhood of these "multi-speed" lattices require that some unknown distribution function have to be recovered away from the wall. A similar approach can be applied here, with the major difference that the velocity is not a known quantity anymore. The boundary conditions for such extended lattices are currently an active research topic and will be adressed in a future paper.

4. Benchmarks

In this section two and three dimensional benchmarks have been implemented in order to test the numerical accuracy of the general regularized boundary condition. The planar 2D Womersley and the square 3D channel flows are compared to the analytical solutions of these flows, and for the case of the self

propelled dipole the present simulations are compared with results obtained in [20] by a high accuracy pseudo-spectral method.

In all these benchmarks, the boundaries are flat walls or corners (in 2D) or flat walls, edges and corners (in 3D). Both are implemented with the method described in the preceding section. The lattice used for the 3D benchmarks is the D3Q19.

The error, E, is computed with

$$E = \sqrt{\frac{1}{M}\sum_i ||\boldsymbol{u}_a(\boldsymbol{x}_i) - \boldsymbol{u}_s(\boldsymbol{x}_i)||^2}, \tag{39}$$

where $\boldsymbol{u}_a$ and $\boldsymbol{u}_s$ stand respectively for the analytical and simulated solutions, the sum is carried out over the M nodes of the computational domain.

4.1. The 2D Womersley flow

The Womersley flow takes place in the same geometry as for the planar channel flow. The main difference is that the flow is driven by a periodic in time pressure gradient. The analytical solution was proposed by Womersley [21]. The amplitude of the pressure oscillations is denoted by A, and the frequency by ω :

$$\partial_x p = -A\cos(\omega t). \tag{40}$$

The Reynolds, $\mathrm{Re} = UL_y/\nu$, number is defined with respect to the characteristic length $L = L_y$ and to the velocity in the middle of the channel when $\omega \to 0$. A second dimensionless parameter is defined to characterize the flow : the Womersley number, α, defined as

$$\alpha = \frac{L_y}{2}\sqrt{\frac{\omega}{\nu}}. \tag{41}$$

With respect to the Reynolds and the Womersley numbers the Womersley profile is given by

$$u_x(y,t) = \mathfrak{Re}\left(\mathrm{e}^{i\frac{\alpha^2}{\mathrm{Re}}t}\frac{8}{i\alpha^2}\left(1 - \frac{\cosh\left(\sqrt{2}(\alpha+i\alpha)\left(y-\frac{1}{2}\right)\right)}{\cosh\left(\frac{\sqrt{2}}{2}(\alpha+i\alpha)\right)}\right)\right), \tag{42}$$

where i is the imaginary unit, and $\mathfrak{Re}$ represent the real part of the expression.

The flow is induced by imposing the analytical profile of Eq. (42) on inlet and on outlet. The error of the Womersley flow is computed as the average over a period of time

$$\langle E\rangle = \frac{1}{T}\sum_j E(t_j), \tag{43}$$

where T is the period and the sum is made over each time-step of a period.

The Reynolds number is taken to be $\mathrm{Re} = 1$, the lattice velocity is set to $U = 0.01$ at a reference resolution of $N = 10$ and $\alpha = 2$. As can be seen on Fig. 3 the error is of order two as expected.

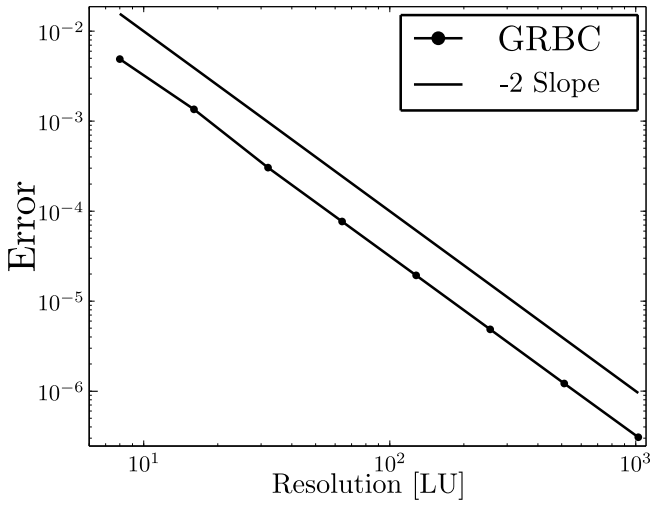

Figure 3: The error of the Womersley solution with respect to the resolution in lattice units.

4.2. The 2D dipole-wall collision

This benchmark, based on Refs. [20] and [22], analyzes the time evolution of a self-propelled dipole confined within a 2D box. The geometry of the box is a square domain $[-L, L] \times [-L, L]$ and is surrounded by no-slip walls. The initial condition describes two counter-rotating monopoles, one with positive core vorticity at the position (x_1, y_1) and the other one with negative core vorticity at (x_2, y_2). This is obtained with an initial velocity field $\boldsymbol{u}_0 = (u_x, u_y)$ which reads as follows in dimensionless variables :

$$u_x = -\frac{1}{2} \|\omega_e\| (y - y_1) \mathrm{e}^{-(r_1/r_0)^2} + \frac{1}{2} \|\omega_e\| (y - y_2) \mathrm{e}^{-(r_2/r_0)^2}, \tag{44}$$

$$u_y = +\frac{1}{2} \|\omega_e\| (x - x_1) \mathrm{e}^{-(r_1/r_0)^2} - \frac{1}{2} \|\omega_e\| (x - x_2) \mathrm{e}^{-(r_2/r_0)^2}. \tag{45}$$

Here, $r_i = \sqrt{(x - x_i)^2 + (y - y_i)^2}$, defines the distance to the monopole centers. The parameter r_0 labels the diameter of a monopole and ω_e its core vorticity.

The average kinetic energy of this system at a given time is defined by the expression

$$\langle E \rangle (t) = \frac{1}{2} \int_{-1}^{1} \int_{-1}^{1} \|\boldsymbol{u}\|^2 (\boldsymbol{x}, t) d^2x, \tag{46}$$

and the average enstrophy by

$$\langle \Omega \rangle (t) = \frac{1}{2} \int_{-1}^{1} \int_{-1}^{1} \omega^2 (\boldsymbol{x}, t) d^2x, \tag{47}$$

where $\omega = \partial_x u_y - \partial_y u_x$ is the flow vorticity.

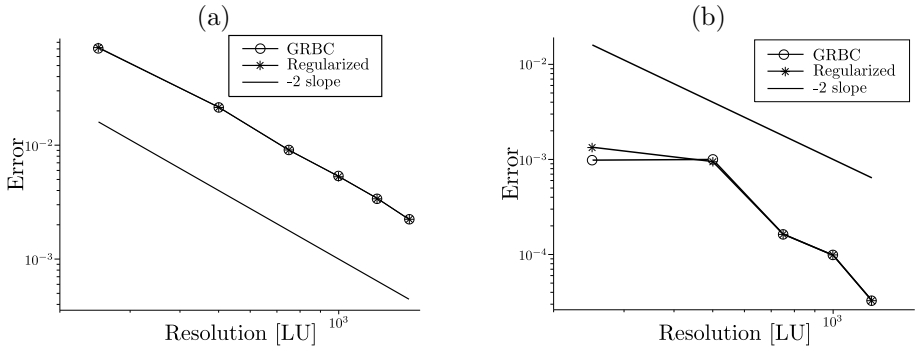

Figure 4: Numerical accuracy in the 2D dipole-wall collision flow for the two enstrophy peaks, (a) $\omega_1 = 933.6$, and (b) $\omega_2 = 305.2$. The error curve for the enstrophy peak obtained with the Regularized BCis also added for comparison purpose.

The dipole described by Eqs. (44) and (45), under the actions of viscous forces, develops a net momentum in the positive x-direction and is self-propelled towards the right wall. The collision between the dipole and the wall is characterized by a turbulent dynamics where the wall acts as a source of small-scale vortices that originate from detached boundary layers. After the first collision the monopoles under the action of viscosity again is re-propelled against the wall. These collisions give rise to two peaks of enstrophy. The value of these local maxima will be used for comparison of our boundary condition with the results obtained with a spectral method in Ref. [20].

In the benchmark, the initial core vorticity of the monopoles is fixed to $\omega_e = 299.5286$, which leads to an initial average kinetic energy of $\bar{E}(0) = 2$. Furthermore, the Reynolds number and the monopole radius are set to $\mathrm{Re} = 625$ and $r_0 = 0.1$. The monopoles are aligned symmetrically with the box, in such a way that the dipole-wall collision is frontal and takes place in the middle of a wall. The position of the monopole centers is $(x_1, y_1) = (0, 0.1)$ and $(x_2, y_2) = (0, -0.1)$. The approach of Ref. [22] is used to set up the initial condition. The initial pressure is evaluated numerically, by solving the Poisson equation with a successive over relaxation (SOR) scheme, using the algorithm described e.g. in Ref. [23]. The off-equilibrium parts of the particle populations are then computed with the help of Eq. (8), with numerically computed velocity gradients. The error, $E_i = (\omega_i - \omega_{i\ \mathrm{lb}})/\omega_i$, ($i = 1, 2$ is the label of the enstrophy peak, and $\omega_{i\ \mathrm{lb}}$ is the value computed with the LBM) is computed with respect to the values found in Ref. [20] : $\omega_1 = 933.6$ and $\omega_2 = 305.2$.

The numerical results in Fig. 4, for a Reynolds number $\mathrm{Re} = 625$, indicate that the GRBC yields the expected second-order accuracy for the first peak and yields indistinguishable results when compared to the Regularized BC. It is striking that the value of the second enstrophy peak is very much more accurately represented than the first one, even when the first peak has a 5% error. It should also be noted that at a resolution of $N = 1500$ the second enstrophy

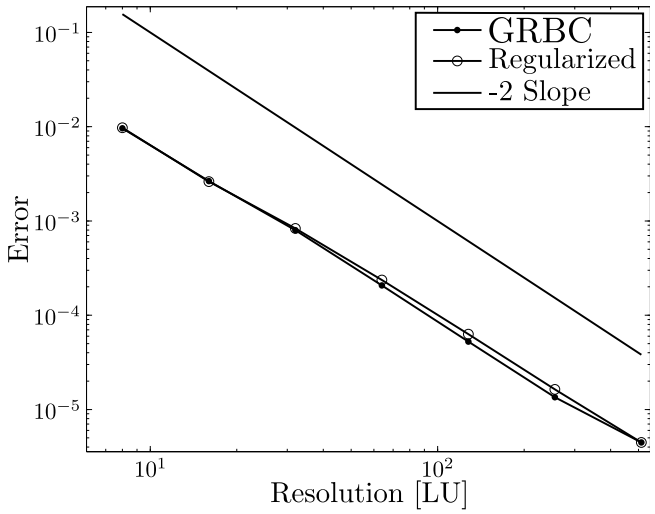

Figure 5: (Numerical accuracy in a 3D channel flow. The error curve of the Regularized BC is also present for comparison purpose.

peak, $\omega_{2\ \mathrm{lb}} = 305.2$, is exactly equal to the value found in [20].

4.3. The 3D square Poiseuille flow

This benchmark describes the steady flow in a 3D rectangular cylinder. The geometry of the channel extends in the z-direction. It has a rectangular cross section, with $x = 0, .., L$ and $y = 0, .., \beta L$ where β is the aspect ratio of the rectangle. The pressure is a linearly decreasing function of z. By symmetry, the only non-null component of the velocity is along the z-direction and is depending only on x and y. The reference velocity U is taken as the maximum velocity in the channel. The pressure drop is the same in the 3D as in the 2D case : $\partial p/\partial z = -8/\mathrm{Re}$. The complete analytic solution to this 3D channel flow is [24]

$$u_z(x,y) = 4(x-x^2) + \frac{32}{\pi^3}\sum_{n=0}^{+\infty}\Bigg(\frac{(-1)^n}{(2n+1)^3} \cos\left((2n+1)\pi x\right)\frac{\cosh\left((2n+1)\frac{\pi y}{\beta}\right)}{\cosh\left((2n+1)\frac{\pi}{2}\beta\right)}\Bigg). \tag{48}$$

Fig. 5 shows the numerical accuracy at $\mathrm{Re} = 10$. The reference velocity is $U = 0.01$ at $N = 50$, and the aspect ratio is $\beta = 1$. The numerical results in this 3D benchmark are similar to those of the 2D application in Sec. 4.1 and the accuracy is again of second order as expected. Furthermore the results are very similar to those obtained with the Regularized BC.

5. Conclusion

In this work we presented a generic way of handling flat walls or corners on boundaries for the lattice Boltzmann method. The boundary conditions were applied in 2D and 3D benchmarks and all of them showed a second order accuracy. Furthermore on two very different benchmark they not only showed to be second order accurate but also to quantitatively give the same results as the Regularized BC. Thanks to the genericity of the procedure, this boundary condition can be applied to lattice Boltzmann method for thermal flows and we are currently working on this adaptation.

[1] S. Succi, The lattice Boltzmann equation for fluid dynamics and beyond, Oxford University Press, Oxford, 2001.

[2] B. Chopard, A. Dupuis, A. Masselot, P. Luthi, Cellular Automata and Lattice Boltzmann techniques: an approach to model and simulate complex systems, Adv. Compl. Sys. 5 (2002) 103–246, doi: 10.1142/S0219525902000602.

[3] O. Malaspinas, Lattice Boltzmann method for the simulation of viscoelastic fluid flows, PhD dissertation, EPFL, Lausanne, Switzerland, URL `http://library.epfl.ch/theses/?nr=4505`, 2009.

[4] X. Shan, H. Chen, Lattice Boltzmann model for simulating flows with multiple phases and components, Phys. Rev. E 47 (1993) 1815–1819, doi: 10.1103/PhysRevE.47.1815.

[5] X. Shan, X.-F. Yuan, H. Chen, Kinetic theory representation of hydrodynamics: a way beyond the Navier Stokes equation, J. Fluid Mech. 550 (2006) 413–441, doi:10.1017/S0022112005008153.

[6] Q. Zou, X. He, On pressure and velocity boundary conditions for the lattice Boltzmann BGK model, Phys. Fluids 9 (1997) 1592–1598.

[7] P. A. Skordos, Initial and boundary conditions for the lattice Boltzmann method, Phys. Rev. E 48 (1993) 4823–4842.

[8] J. Latt, B. Chopard, Lattice Boltzmann Method with regularized non-equilibrium distribution functions, Math. Comp. Sim. 72 (2006) 165–168.

[9] J. C. G. Verschaeve, Analysis of the lattice Boltzmann Bhatnagar-Gross-Krook no-slip boundary condition: Ways to improve accuracy and stability, Phys. Rev. E 80 (3) (2009) 036703, doi:10.1103/PhysRevE.80.036703.

[10] J. Latt, B. Chopard, O. Malaspinas, M. Deville, A. Michler, Straight velocity boundaries in the lattice Boltzmann method, Phys. Rev. E 77 (5) (2008) 056703–+, doi:10.1103/PhysRevE.77.056703.

[11] M. Bouzidi, M. Firdaouss, P. Lallemand, Momentum transfer of a Boltzmann-lattice fluid with boundaries, Phys. Fluids 13 (11) (2001) 3452–3459, doi:10.1063/1.1399290.

[12] M. Junk, Z. Yang, One-point boundary condition for the lattice Boltzmann method, Phys. Rev. E 72 (6) (2005) 066701, doi: 10.1103/PhysRevE.72.066701.

[13] I. Ginzburg, D. d'Humières, Multireflection boundary conditions for lattice Boltzmann models, Phys. Rev. E 68 (6) (2003) 066614, doi: 10.1103/PhysRevE.68.066614.

[14] D. A. Wolf-Gladrow, Lattice-Gas Cellular Automata and Lattice Boltzmann Models: An Introduction, Springer-Verlag, Berlin, 2000.

[15] P. L. Bhatnagar, E. P. Gross, M. Krook, A Model for Collision Processes in Gases. I. Small Amplitude Processes in Charged and Neutral One-Component Systems, Phys. Rev. 94 (3) (1954) 511–525, doi: 10.1103/PhysRev.94.511.

[16] S. Chapman, T. G. Cowling, The mathematical theory of nonuniform gases, Cambridge University Press, Cambridge, 1960.

[17] B. Chopard, M. Droz, Cellular Automata Modeling of Physical Systems, Cambridge University Press, 1998.

[18] K. Huang, Statistical Mechanics, J. Wiley, New York, 1987.

[19] Å. Björck, Numerical Methods for Least Squares Problems, SIAM, Philadelphia, 1996.

[20] H. J. H. Clercx, C.-H. Bruneau, The normal and oblique collision of a dipole with a no-slip boundary, Comput. Fluids 35 (2006) 245–279.

[21] J. R. Womersley, Method for the calculation of velocity, rate of flow and viscous drag in arteries when the pressure gradient is known, J. Physiol. 127 (1955) 553–563.

[22] J. Latt, B. Chopard, A benchmark case for lattice Boltzmann: turbulent dipole-wall collision, Int. J. Mod. Phys. C 18 (2007) 619–626.

[23] M. Griebel, T. Dornseifer, T. Neunhoeffer, Numerical simulation in fluid dynamics: a practical introduction, Society for Industrial and Applied Mathematics, Philadelphia, PA, USA, ISBN 0-89871-398-6, 1998.

[24] C.-S. Yih, Fluid Mechanics, McGraw-Hill, London, 1969.